# X-ray Diffraction Analysis of Severely Cold Deformed Hypereutectoid Steel Wire

S.S. Bargujer[*,#], N.M. Suri[#], and R.M. Belokar[#]

*Ordnance Cable Factory, Chandigarh - 160 002, India*
#*PEC University of Technology, Chandigarh - 160 012, India*
*E-mail: bargujer@yahoo.com*

## ABSTRACT

Hypereutectoid steel wire rod of diameter 6.40 mm is lead patented in lead bath of an electric powered furnace and then it is cold drawn through converging conical dies in a die sequence up to 2.50 mm diameter. The drawn wires subjected to different true strain are analysed using line profile X-ray diffraction methods. The classical Williamson-Hall plot as well as modified Williamson-Hall plot of drawn wire specimens of different true strain is plotted. The theoretical as well as experimental value of $q$ is evaluated. The $q$ is a parameter which depends up on elastic constant of the crystal and type of dislocations. The changes in nature of dislocations from edge dislocations to screw dislocations are calculated against true strain and are verified by scanned electron microscopy's micrograph of drawn wire.

**Keywords:** Hypereutectoid steel wire, Williamson-Hall plot, spring, true strain, x-ray diffraction, elastic constant and full width half maximum, FWHM

## 1. INTRODUCTION

The detailed study on lead patenting and wire drawing of pearlitic steel wire[1-2] has been carried out by analysing SEM/TEM micrograph but limited study has been reported on hypereutectoid steel wire drawing process by X-ray diffraction (XRD) methods so far. XRD analysis has been done on Cu[3-7], ferritic-pearlitic steel[8], Aluminium[9-10] martensitic steel[11-12], pearlitic steel[13-15], nickle[16], FeN[17], 10Cr-5W heat resistant steels[18]. The elaborate study on elastic constants[19] for hypereutectoid steel and dislocations contrast factors[20-22] of cubic crystals is available in literature. The present study is carried out to correlate the mechanical properties, microstructural changes as well as detailed X-ray diffraction line profile analysis for better understanding of cold drawing process of hypereutectoid steel wires.

The springs[23] are used in the arms and ammunitions[24] for performing specific task. A few example of application of hypereutectoid steel wire which are used for manufacturing springs are of diameter 0.35 mm, 0.45 mm, 0.50 mm, 0.60 mm, 0.70 mm, 0.90 mm, 1.00 mm, 1.20 mm, 1.25 mm, 1.30 mm, 1.40 mm, 1.50 mm, 2.00 mm, 2.30mm, 2.50 mm, 2.80 mm, 3.00 mm, 4.50 mm and 5.00 mm. These wires are used in various springs for 0.22″ revolver, 0.32″ pistol, 5.56 mm INSAS rifle, 30-06 sporting rifle, tear gas gun, MCIWS weapon, pump action gun, double barrel breach loading gun, 7.62 mm rifle, 12.7 mm AD gun, ILG gun, PRG gun, and 30 mm Cannon, T-72 Tank gun, etc.

The lead patented hypereutectoid steel wire has a very fine alternate layer of ferrite and cementite lamellae. These alternate layers in fine pearlite cannot be resolved under optical microscope. Hypereutectoid steel wire does not have any cementite network on its grain boundary. The lamellas of ferrite and cementite have same orientation in individual pearlite colony but each pearlite colony has different and random orientation of lamellas from its neighbour's pearlite colonies. The hypereutectoid steel wire has higher ultimate tensile strength (UTS) and torsion strength as compared to other steel.

## 2. EXPERIMENTAL WORK

The chemical composition of hypereutectoid steel wire rod used in the study is mentioned in Table 1. The initial diameter of lead patented wire rod is 6.40 mm. The sample is subjected to cold wire drawing process and mechanical properties are recorded after drawing from each die. The results are mentioned in Table 2. The selected samples for X-ray analysis are of 6.40 mm, 5.80 mm, 5.30 mm, 4.40 mm, 3.60 mm, 3.0 mm, and 2.50 mm diameter.

**Table 1. Chemical composition of wire rod**

| Carbon | Manganese | Silicon | Sulphur | Phosphorous |
|--------|-----------|---------|---------|-------------|
| 0.88 | 0.48 | 0.20 | 0.005 | 0.006 |

The plot of ultimate tensile strength (UTS) vs. true strain for drawn sample is shown in Fig. 1(a). The bar chart indicating the contribution percentage in the gain of UTS of wires by lead patenting process and wire drawing process are shown in Fig. 1(b). The Fig. 1(c) show the swirling of lamellar structure due to wire drawing strain. The average grain size number of lead patented wire rod of diameter 6.40 mm is 9.5. The average grain size number is calculated using optical microscopic image by standard method.

**Table 2. Draw dies sequence of wire**

| Diameter of wire | Ultimate tensile strength (MPa) | Ultimate torsion strength (nos. of turn) |
|---|---|---|
| 6.4 | 1378.34 | 24 |
| 5.8 | 1486.84 | 26 |
| 5.3 | 1531.1 | 28 |
| 4.8 | 1592.09 | 28 |
| 4.4 | 1599.73 | 26 |
| 4.0 | 1742.35 | 40 |
| 3.6 | 1777.73 | 24 |
| 3.3 | 1870.03 | 23 |
| 3.0 | 1896.18 | 25 |
| 2.7 | 2004.13 | 24 |
| 2.5 | 2069.1 | 25 |

## 3. RESULTS AND DISCUSSION

The X-ray diffraction line profile analysis is done by Philip PAN XPRT analysis X-ray diffraction (XRD) machine having copper as X-ray generating source. The W. H. Bragg carried out experimentation on X-ray diffraction of various materials and found that the incident beam, the normal to diffraction plane and the transmitted beam are always coplanar. The angle between the diffracted beam and the transmitted beam is always twice of the diffraction angle. According to Bragg's law: $d = \lambda/2\sin\theta$. Where, $d$ is inter-planer spacing, normally called as $d$-spacing, $\lambda$ is wavelength of X-rays and $\theta$ is diffraction angle. XRD of a pearlitic steel wire mainly display peak generated from ferrite phase. The XRD graphs of samples subjected to various degree of cold working are as shown in Fig. 2 (a) - 2(e).

### 3.1 X-ray Peak Analysis

Peaks in XRD plots are identified by using Bragg's law

and crystal geometry of ferrite phase of steel. In b.c.c. crystal, $d_{hkl}$ of an $hkl$ plane = $a/(h^2+k^2+l^2)^{1/2}$. Where, a is unit cell dimension and is equal to $4 r/(3)^{1/2}$. Where, $r$ is atomic radius of ferrite. The indexing of diffraction peaks is done on the basis of structural factor using equation $\lambda/4a^2 = \sin\theta_{hkl}/(h^2+k^2+l^2)$ = constant. For b.c.c. crystals, those diffraction planes which satisfies the condition $h+k+l$ = even are only producer of the constructive peaks in XRD.

The plot of FWHM vs. true strain for different diffraction planes is shown in Fig. 3. The plot indicates that FWHM increases almost linearly with increase in true strain although rate of increase is slightly differ from plane to plane as indicated in Fig. 3. The maximum increase in FWHM is noticed at 310 diffraction plane.

The broadening of diffraction lines due to non-uniformity of strain is obtained by the Bragg's law as: $b = - 2(\Delta d/d)\ tan\theta$. Where $b$ is broadening due to fractional variation in Bragg plane spacing, $\Delta d/d$. When a heat treated metal is cold worked, its diffraction lines become broader. The broadening of diffraction lines is due to particle size or due to strain becomes a point of controversy. The separation of the size and strain components can be done by plotting $B\ Cos\theta$ as a function of $Sin\theta$. Where, $B$ is FWHM of a peak. This plot of $B\ Cos\theta$ vs. $Sin\theta$ is known as classical Williamson-Hall plot and implicitly assumes that peak shapes are Lorentzian.

### 3.2 The Classical Williamson-Hall Plot

The classical Williamson-Hall plot for steel wire samples are plotted at different true strain in Fig. 4 (a) - 4(g). In a classical Williamson-Hall plot, X-axis represents $B\ (Cos\theta)/\lambda$ and Y-axis represents $Sin\theta/\lambda$. The Scherrer equation can be used to find out the broadening of peak width due to crystallite size or strain broadening. The Scherrer equation is as: $B\ Cos\theta = K\ \lambda / L + 4\ \varepsilon\ Sin\theta$. Where, first part of equation indicates the role of crystallite size in broadening of peak and the value of
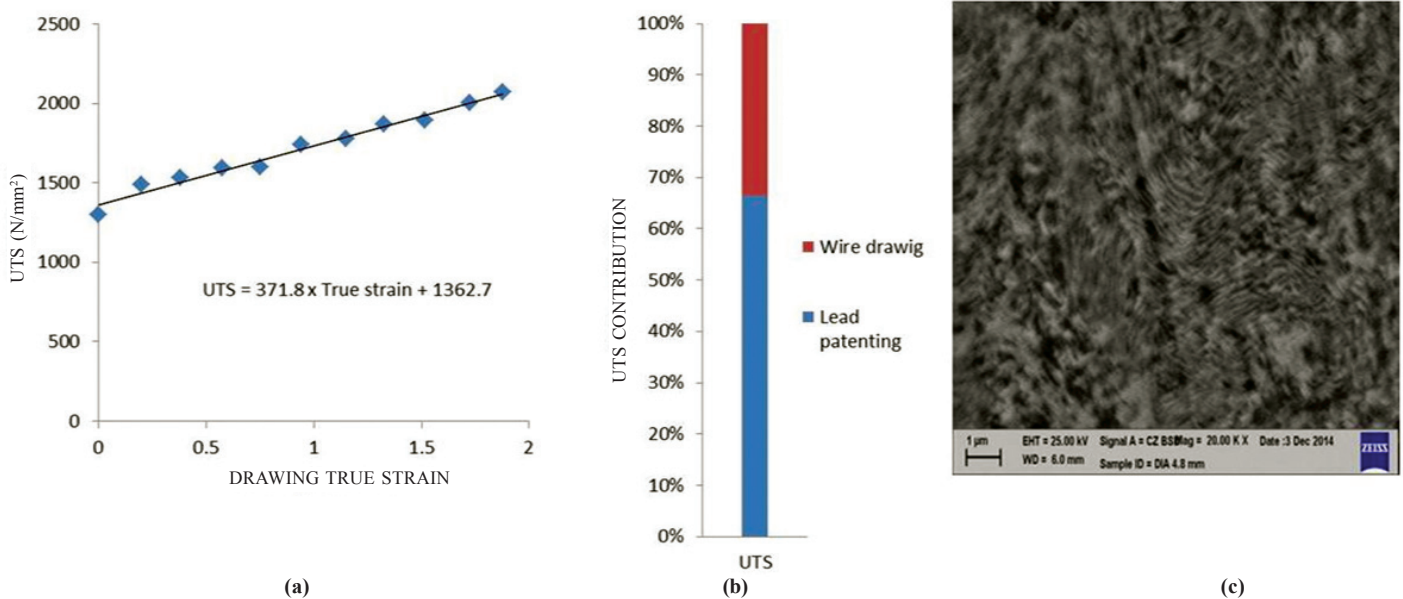


**Figure 1.** (a) UTS vs drawing true strain plot, (b) Bar chart shows the contribution of lead patenting process and wire drawing process in UTS of wire, and (c) SEM micrograph showing the dominance of swirling of lamellar at 0.5753 drawing true strain, respectively.
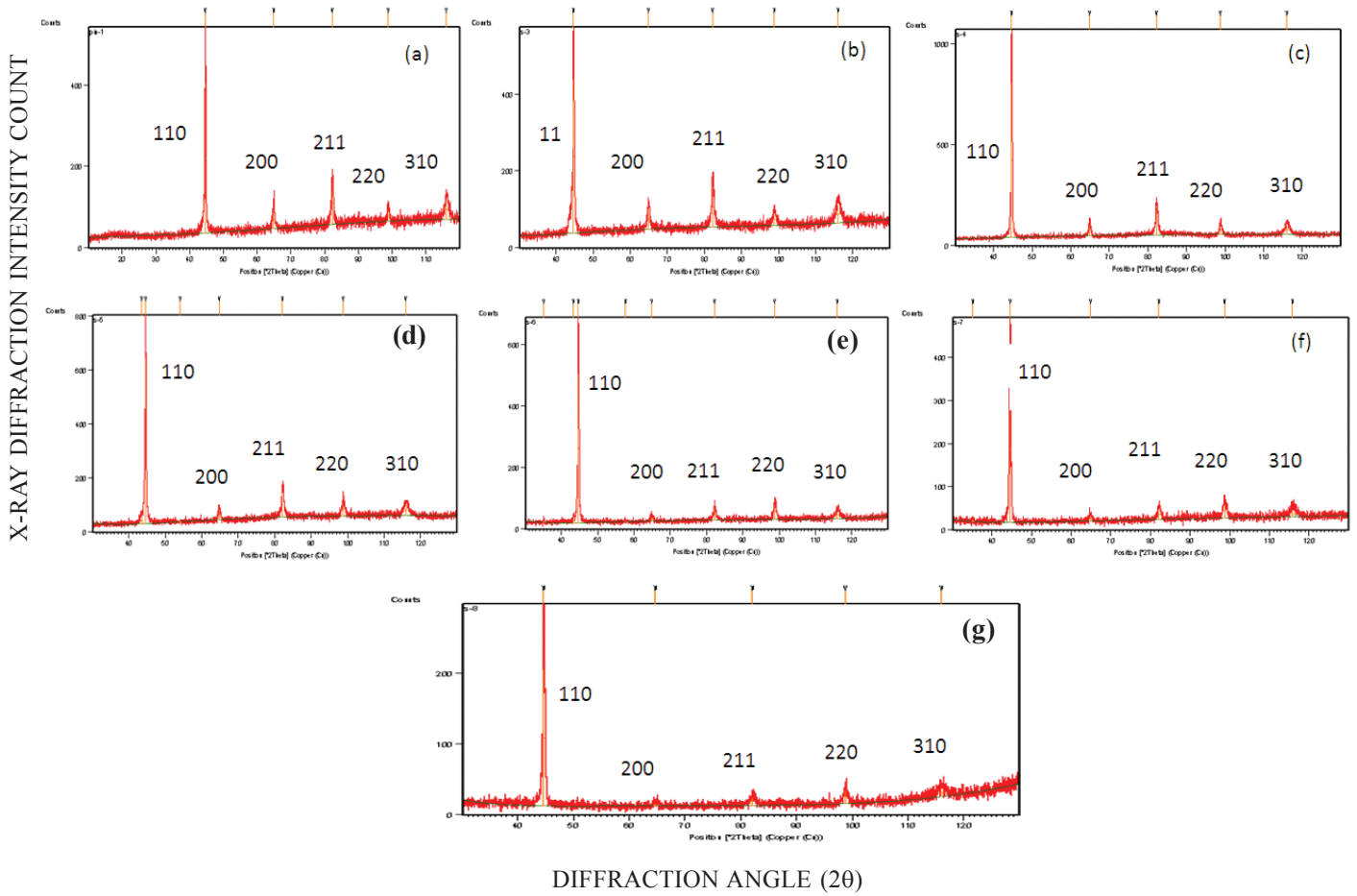
**Figure 2. (a)-(g): X-ray diffraction line profile of 6.40 mm, 5.80 mm, 5.30 mm, 4.40 mm, 3.60 mm and 3.00 mm, and 2.50 mm diameter wire, respectively.**
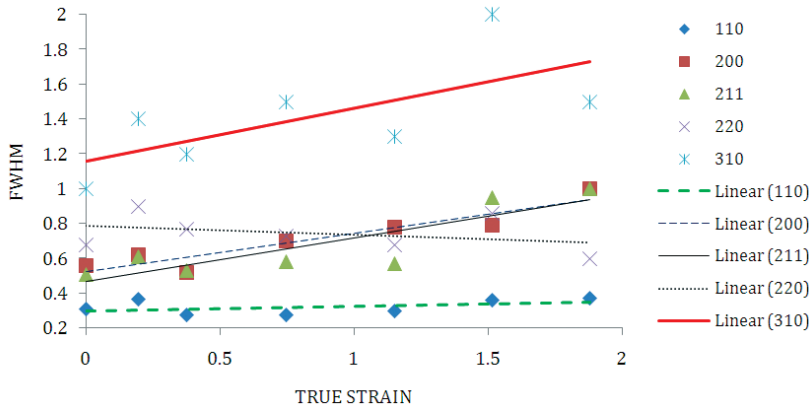


**Figure 3. FWHM vs. true strain plot for plane having 110, 200, 211, 220 and 310 diffraction planes.**

this part is given by linear interception on $Y$ axis. The second part of equation indicates the role of strain in broadening of peak and is equal to slope of linear plot. The crystallite size is calculated using data from XRD figures with the help of Scherrer equation. The crystallite size is 57.32 nm, 56.679 nm, 52.51 nm, 43.57 nm and 42.21 nm at drawn true strain nil, 0.743, 1.150, 1.515, and 1.880, respectively. This indicates that the increase in drawn true strain results in decrease in crystallite size.

According to Modified Williamson-Hall equation, the line broadening of diffraction profile with increasing diffraction order is caused by dislocations in strain anisotropy. The FWHM of the diffraction profile as per modified Williamson-hall plot is:

$$\Delta K \sim= \gamma/d + (\pi\, M^2 b^2)/2 * \rho^{1/2} * K^2 C + O\,(K^4 C^2)$$

where $\gamma = 0.90$ for ferrite. $d$ = size parameter. $\rho$ = average dislocation density. $b$ = length of Burgur's vector of dislocation and is equal to 0.248 nm for pearlitic steel. $M$ = a constant which depends upon effective outer cut-off radius of dislocation and is determined from Fourier coefficient. $C$ = contrast factor of dislocation. $O$ = higher order term in $K^4 C^2$. $\Delta K = Cos\,\theta\,[\Delta\,(2\theta)]/\lambda$, where $\Delta\,(2\theta)$ is FWHM of diffraction peak and $H^2 = (h^2 k^2 + h^2 l^2 + k^2 l^2)/(h^2 + k^2 + l^2)$.

Average dislocation contrast factor of un-textured cubic polycrystalline $C = C_{h00}(1-qH^2)$, where $C_{h00}$ is average

**Table 3. $C_{pure\ edge}$ and $C_{pure\ screw}$ for different diffraction plane $g$**

| $g$ | (110), (220) | (200) | (211) | (310) |
|---|---|---|---|---|
| $C_{pure\ edge}$ | 0.1795 | 0.1861 | 0.1795 | 0.1837 |
| $C_{pure\ screw}$ | 0.1057 | 0.2522 | 0.1056 | 0.0758 |

dislocation contrast factor for *h00* reflections. *q* is a parameter which depends up on elastic constant of the crystal and type of dislocations, i.e., edge or screw dislocations. The contrast factors $C_{h00}$ for different diffraction vector *g* for pure edge dislocations and pure screw dislocations of ferrite is calculated using ANZIC software and are mentioned in Table 3.

### 3.3 Theoretical Methods for Determination of *q*

The value of *q* is a function of elastic constants of steel. The average polycrystalline elastic constants for α-Fe are taken from Kim[19], *et al*. The values of $c_{11}$, $c_{12}$, $c_{44}$ for hypereutectoid steel are 231.5 GPa, 135.0 GPa, and 116.0 GPa, respectively. The theoretical value of *q* is determined by using Eqn (9).
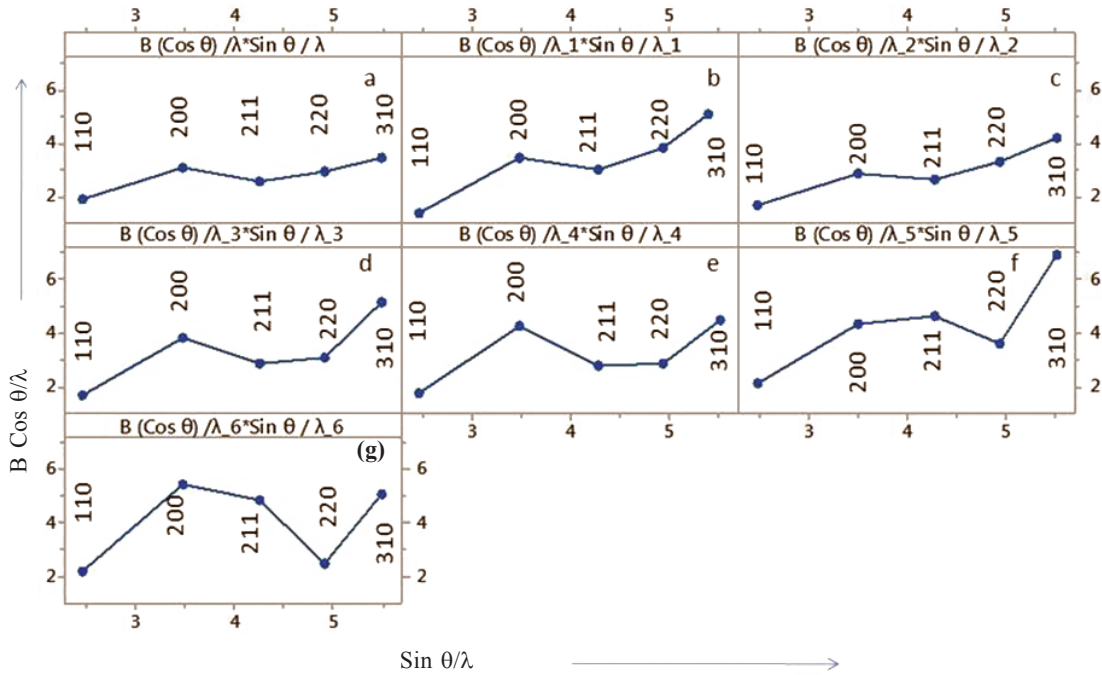


Figure 4. (a)-(g): The classical Williamson-Hall plot for hypereutectoid steel wire as lead patented and at 0.1968, 0.3771, 0.7493, 1.1507, 1.5153, and 1.8800 true strain, respectively.
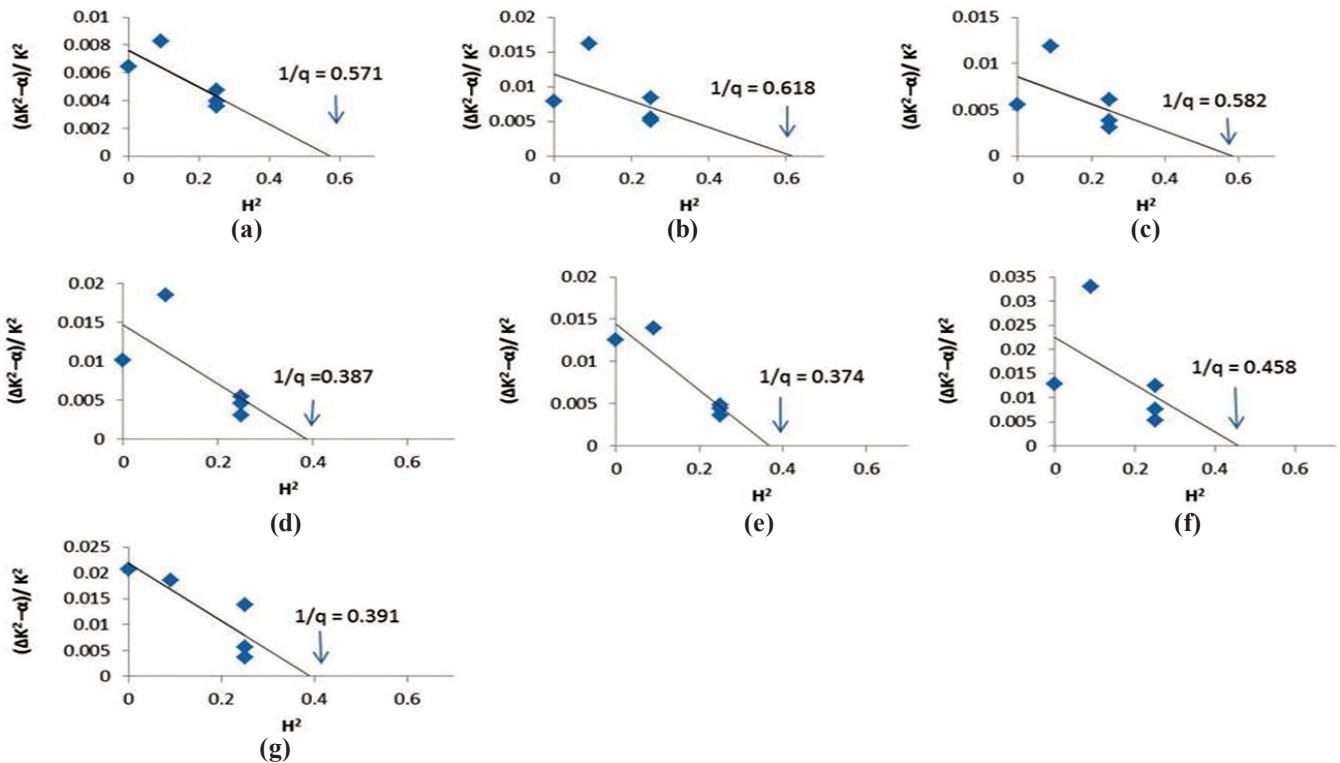


Figure 5. (a)-(g): Experimental value of *q* for hypereutectoid steel wire drawn to true strain of 0.00, 0.1968, 0.3771, 0.7493, 1.1507, 1.5153, and 1.8800 with average crystallite size 70 nm, 63 nm, 57 nm, 48 nm, 39 nm, 32 nm, and 27 nm are 1.750, 1.618, 1.717, 2.578, 2.669, 2.183, and 2.555, respectively.

**Table 4.    The parameters *a, b, c, d* for $c_{12}/c_{44}$ ratio equal to 1 and 2**

| Type of dislocation | $c_{12}/c_{44}$ | a | b | c | d |
|---|---|---|---|---|---|
| Screw | 1 | 8.6590 | 0.3730 | 0.0424 | -6.074 |
| Screw | 2 | 6.0725 | 0.4338 | 0.0415 | -3.5021 |
| Edge | 1 | 7.2361 | 0.9285 | 0.1359 | -5.7484 |
| Edge | 2 | 8.8331 | 0.8241 | 0.1078 | -7.0570 |

**Table 5.    The calculated value of $q_{screw}$ and $q_{edge}$ for different ratio $c_{12}/c_{44}$**

| $A_i$ | $c_{12}/c_{44}$ | $q_{screw}$ | $q_{edge}$ |
|---|---|---|---|
| 2.416 | 1 | 2.674 | 1.280 |
| 2.416 | 2 | 2.647 | 1.783 |
| 2.416 | 1.163 | 2.669 | 1.362 |

$q = a[1- exp.(-A_i/b)] + cA_i + d$. (T. Ungar[20] et. al.).
where, $A_i$ is a Zener constant, which depends upon the elastic constant and $A_i = 2c_{44}/(c_{11}-c_{22})$. The value of parameters *a, b, c, d* for above equation are taken from Table 8 and 9 of Ungar[20], et. al. and the same are reproduced in Table 4. The calculated values of *q* in case of screw dislocations and edge dislocations in b.c.c. crystal system are mentioned in Table 5.

## 3.4  Experimental Methods for Determination of *q*

The experimental method used for determination of *q* is based on equation 12 proposed by Ungar[20], et.al. are shown in Fig. 5(a-g). The equation is $[(\Delta K)^2-\alpha]/K^2 = \beta C_{h00}(1-qH^2)$. Where, $\alpha = (0.9/D)^2$ and $\beta = \pi M^2 b^2 \rho/2$. *D* is average particle size. *M* is a constant which depends on the effective outer cut off radius of dislocations. $K = 2 \sin\theta/\lambda$, $\Delta K$ is FWHM. The interception point on x-axis by best regression line gives the value of $1/q$.

## 3.5  Evaluation of $C_{actual}$ by using $q_{exp}$

The $C_{actual}$ is calculated by using simple lever rule with $q_{exp.}, q_{th}^{edge}$ and $q_{th}^{Screw}$ and are mentioned in Table 6.

## 3.6  Modified Williamson- Hall Plots

The modified Williamson- Hall plots predicts that if strain broadening of diffraction profile in drawn steel wires is caused by dislocations then $(KC)^{1/2}$ will have binomial relationship with FWHM. The modified Williamson- Hall plots of hypereutectoid steel wires at different true strain are shown in Fig. 6 (a-g). The slope of modified Williamson-Hall plot shows an increasing trend from Fig. 6(a) to 6(g). This demonstrates that the numbers of dislocations increases with increase in true strain.

The character of prevailing dislocation can be described using equation 7 of Movaghar Garabagh[12], et. al. as: $f^{edge} = 1 - f^{screw} = (q_{th}^{Screw} - q_{exp})/(q_{th}^{Screw} - q_{th}^{edge})$. Where, $f^{edge}$ and $f^{screw}$ is fraction of edge and screw type dislocations respectively. $q_{th}^{Screw}$ and $q_{th}^{edge}$ is theoretical *q* value for screw and edge type dislocations respectively. $q_{exp}$ is experimental value of *q*. The fraction of pure edge dislocations and pure screw dislocations at various true drawn strains are mentioned in Table 7.

Initially the value of $q_{exp}$ shows an increasing trend till

**Table 6.    The calculated value $C_{actual}$ of for different true strain and diffraction plane**

| Wire diameter (in mm) | True strain | $q_{exp}$ | Diffraction plane | $c_{pure\ edge}$ | $c_{pure\ screw}$ | $c_{actual}$ |
|---|---|---|---|---|---|---|
| 6.40 | 0.00 | 1.750 | 110 | 0.1795 | 0.1057 | 0.1576 |
| | | | 200 | 0.1861 | 0.2522 | 0.2056 |
| | | | 211 | 0.1795 | 0.1056 | 0.1575 |
| | | | 220 | 0.1795 | 0.1057 | 0.1576 |
| | | | 310 | 0.1837 | 0.1995 | 0.1883 |
| 5.80 | 0.1968 | 1.618 | 110 | 0.1795 | 0.1057 | 0.1650 |
| | | | 200 | 0.1861 | 0.2522 | 0.1990 |
| | | | 211 | 0.1795 | 0.1056 | 0.1650 |
| | | | 220 | 0.1795 | 0.1057 | 0.1650 |
| | | | 310 | 0.1837 | 0.1995 | 0.1867 |
| 5.30 | 0.3771 | 1.717 | 110 | 0.1795 | 0.1057 | 0.1594 |
| | | | 200 | 0.1861 | 0.2522 | 0.2040 |
| | | | 211 | 0.1795 | 0.1056 | 0.1594 |
| | | | 220 | 0.1795 | 0.1057 | 0.1594 |
| | | | 310 | 0.1837 | 0.1995 | 0.1879 |
| 4.40 | 0.7493 | 2.578 | 110 | 0.1795 | 0.1057 | 0.1108 |
| | | | 200 | 0.1861 | 0.2522 | 0.2475 |
| | | | 211 | 0.1795 | 0.1056 | 0.1107 |
| | | | 220 | 0.1795 | 0.1057 | 0.1108 |
| | | | 310 | 0.1837 | 0.1995 | 0.1983 |
| 3.60 | 1.1507 | 2.669 | 110 | 0.1795 | 0.1057 | 0.1057 |
| | | | 200 | 0.1861 | 0.2522 | 0.2521 |
| | | | 211 | 0.1795 | 0.1056 | 0.1056 |
| | | | 220 | 0.1795 | 0.1057 | 0.1057 |
| | | | 310 | 0.1837 | 0.1995 | 0.1994 |
| 3.00 | 1.5153 | 2.183 | 110 | 0.1795 | 0.1057 | 0.1331 |
| | | | 200 | 0.1861 | 0.2522 | 0.2275 |
| | | | 211 | 0.1795 | 0.1056 | 0.1331 |
| | | | 220 | 0.1795 | 0.1057 | 0.1331 |
| | | | 310 | 0.1837 | 0.1995 | 0.1936 |
| 2.50 | 1.8800 | 2.555 | 110 | 0.1795 | 0.1057 | 0.1121 |
| | | | 200 | 0.1861 | 0.2522 | 0.2464 |
| | | | 211 | 0.1795 | 0.1056 | 0.1120 |
| | | | 220 | 0.1795 | 0.1057 | 0.1121 |
| | | | 310 | 0.1837 | 0.1995 | 0.1981 |

maxima is achieved then slightly decreases trend as shown by dotted line in the Fig. 7. The SEM micrograph shown in Fig. 1(c) and Fig. 7 confirms that the screw dislocations increase initially till maxima is achieved with increase in true strain and then slightly decreases.
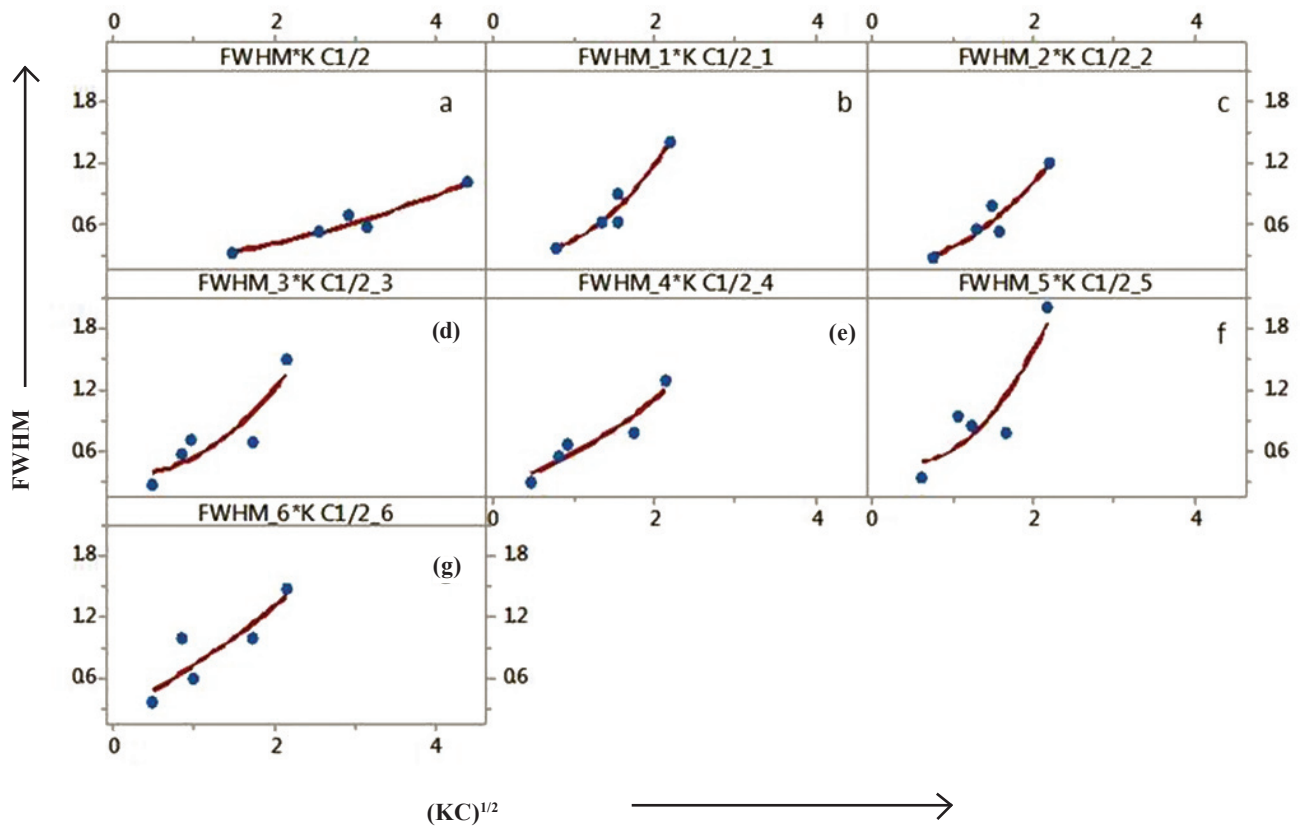
**Figure 6. (a)-(g): The Modified Williamson-hall plot for hypereutectoid steel wire as lead patented and at 0.1968, 0.3771, 0.7493, 1.1507, 1.5153, and 1.8800 true strain, respectively.**

**Table 7. The fraction of pure edge and pure screw dislocations at different true strain**

| Wire diameter | True drawn strain | $q_{exp}$ | $q_{th}^{edge}$ | $q_{th}^{Screw}$ | $f^{edge}$ | $f^{screw}$ |
|---|---|---|---|---|---|---|
| 6.40 | 0.0000 | 1.750 | 1.362 | 2.669 | 0.7035 | 0.2964 |
| 5.80 | 0.1968 | 1.618 | 1.362 | 2.669 | 0.8044 | 0.1955 |
| 5.30 | 0.3771 | 1.717 | 1.362 | 2.669 | 0.7287 | 0.2712 |
| 4.40 | 0.7493 | 2.578 | 1.362 | 2.669 | 0.0701 | 0.9298 |
| 3.60 | 1.1507 | 2.660 | 1.362 | 2.669 | 0.0005 | 0.9994 |
| 3.00 | 1.5153 | 2.183 | 1.362 | 2.669 | 0.3722 | 0.6277 |
| 2.50 | 1.8800 | 2.555 | 1.362 | 2.669 | 0.0877 | 0.9122 |
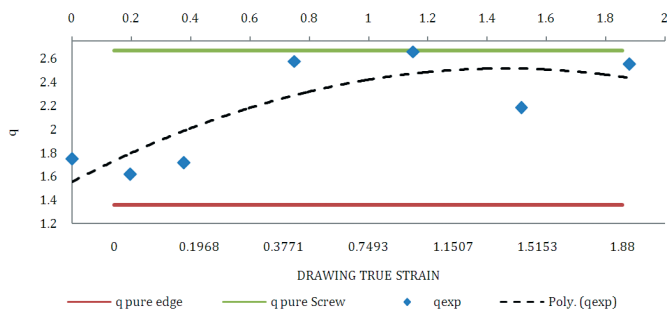


**Figure 7. The plot of $q_{exp}$, $q_{pure\ edge}$ and $q_{pure\ screw}$ vs drawing true strain along with trend line for $q_{exp}$.**

## 4. CONCLUSION

The tensile strength of patented drawn wires increases linearly with increase in true strain as: UTS = 371.8 x True strain + 1362.7. Approximately 66 percent of total UTS are gained by lead patenting process and 34 percent of total UTS are gained by wire drawing process. The drawn wire sample shows that FWHM of the peaks increases with increase in true strain. The classical Williamson-Hall plot of drawn wire specimens shows that broadening of peaks are due to drawing true strain as well as fine microstructure of hypereutectoid steel wire. The value of $q$ by experimental method shows good agreements with theoretical method. The exact contribution of edge and screw dislocations in $q$ value has been found out with increasing drawn true strain. It is observed that with increase in drawn true strain, there is increase in screw type dislocations and reductions in edge type dislocations till approximately 1.515 drawn true strain. After that a marginal decrease in screw type dislocations and increases in edge type dislocations with further increases in strain. The modified Williamson-Hall plot of drawn wire specimens shows that strain anisotropy in drawn samples is mainly due to dislocations.

## REFERERCES

1. Elwazri, A.M.; Wanjara, P. & Yue, S. The effect of microstructure characteristics of pearlite on the mechanical properties of hypereutectoid steel. *Mater. Sci. Eng. A,* 2005, **404**, 91-98.
doi: 10.1016/j.msea.2005.05.051.

2. Zhang, X.; Godfrey, A.; Huang, X.; Hansen, N. & Liu, Q. Microstructure and strengthening mechanisms in cold-drawn pearlitic steel wire. *Acta Materialia*, 2011, **59**, 3422-3430.
doi: 10.1016/j.actamat.2011.02.017.

3. Ungar, T.; Gubicza, J.; Rabarik, G. & Borebely, A. Crystallite size distribution and dislocation structure determined by diffraction profile analysis: principles and practical application to cubic and hexagonal crystals. *J. Appl. Crystallography*, 2001, **34**,298-310.
doi: 10.1107/S0021889801003715.

4. Ungar, T.; Gubicza, J.; Hanak, P. & Alexandrov, I. Densities and character of dislocations and size-distribution of sub grain in deformed metal by X-ray diffraction profile analysis. *Mater. Sci. Eng. A*, 2001, **319-321**, 274-278.
doi: 10.1016/S0921-5093(01)01025-5.

5. Gubicza, J.; Rabarik, G.; Goren-Muginstein, G.R.; Rosen, A.R. & Ungar, T. The density and the character of dislocations in cubic and hexagonal polycrystals determined by X-ray diffraction. *Mater. Sci. Eng. A*, 2001, **309-310**, 60-63.
doi: 10.1016/S0921-5093(00)01666-X.

6. Dragomir-Cernatescu, I.; Gheorghe, M.; Thadhani, N. & Snyder, R. L. Dislocation densities and character evolution in copper deformed by rolling under liquid nitrogen from X-ray peak profile analysis. JCPDS-International Centre for Diffraction Data, Advance in X-ray Analysis, 2005, **48**, 67-72.
doi:10.1524/zksu.2008.0013.

7. Ungar, T.; Ott, S.; Borbely, A. & Weertman, J. R. Dislocations, grain size and planar faults in nanostructured copper determined by high resolution X-ray diffraction and a new procedure of peak profile analysis. *Acta Materialia*, 1998, **46**(12), 3693-3699.
doi: 10.1016/S1359-6454(98)00001-9.

8. Simek, D.; Rafaja, D.; Motylenko, Klemm, V.; Ullrich, C.; Oswald, A. & Schmidtchen, R. The exploitation of X-ray diffraction in characterization of strength of hot-rolled and cold-drawn ferritic-pearlitic steel. *Mater. Struct.*, 2011, **18** (3), 178-183.

9. Goodarzy, M.H.; Arabi, H.; Boutorabi, M.A.; Seyedein, S.H. & Shahrokhi, H. Dislocations structure and scattering phenomenon in crystalline cell size 2024 AL alloy deformed by one pass ECAP at room temperature. *Iranian J. Mater. Sci. Eng.*, 2014, **11**(1), 27-38.
doi: 10.1016/S1003-6326(14)63245-3.

10. Rezvanifar, A. & Zandrahimi, M. Evaluation of dislocation structure and crystallite size in worn AL –SI alloy by X-ray diffraction. *Iranian J. Mater. Sci. Eng.*, 2010, **7**(1), 32-38.

11. Takebayashi, S.; Kunieda, T.; Yoshinaga, N.; Ushioda, K. & Ogata, S. Comparison of the dislocation density in martensitic steels evaluated by some X-ray diffraction methods. *ISIJ International*, 2010, **50** (6), 875-882.
doi.org/10.2355/isijinternational. 50.875.

12. Garabagh, M.R.M.; Nedjad, S.H.; Shirazi, H.; Mobarekeh, M.I. & Ahmadabadi, M.N. X-ray diffraction peak profile analysis aiming at better understanding of the deformation process and deformed structure of a martensitic steel. *Thin Solid Films*, 2008, **516**, 8117-8124.
doi:10.1016/j.tsf.2008.04.019.

13. Kriska, M.; Tacq, J.; Acker, K.V.; Seefeldt, M. & Petegem, S.V. Neutron and X-ray diffraction study of residual and internal stress evolution in pearlitic steel during cold drawing. *J. Phy.*, Conference Series, 2012, **340**, 1-7.
doi:10.1088/1742-6596/340/1/012101.

14. Sato, S.; Wagatsuma, K.; Ishikuro, M.; Kwon, E.-P.; Tashiro, H. & Suzki, S. Precise characterization of dislocations and cementite in pearlitic steels at different drawing strains using X-ray diffraction. *ISIJ International*, 2013, **53**(4), 673-679.
doi: 10.2355/isijinternational.53.673.

15. Chakarborty, J.; Maiti, T.; Ghosh, M.; Das, G. & Chandra, S. Cementite dissolution in cold drawn pearlitic steel wires: role of dislocations. *Mater. Sci. Forum*, 2014, **768-769**, 304-312.
doi: 10.4028/www.scientific.net/MSF.768-769.304.

16. Kamminga, J.-D. & Seijbel, L.J. Diffraction line broadening analysis if broadening is caused by both dislocations and limited crystallite size. *J. Res. National Inst. Standard Technol.* 2004, **109**, 65-74.
doi:10.6028/ jres.109.005

17. Leineweber, A. & Mittemeijer, E. J. Anisotropic strain-like broadening due to composition variations. JCPDS – International Centre for Diffraction Data, Advances in X-ray Analysis, 2003,**46**, 43-48.
doi:10.1.1.296.962

18. Cong, Z. & Murata, Y. Dislocation density of lath martensite in 10Cr-5W heat resistant steels. *Mater. Trans.*, 2011, **52**(12), 2151-2154.
doi: 10.2320/ matertrans.M2011201.

19. Kim, S.A. & Johnson, W.L. Elastic constants and internal friction of martensitic steel, ferritic-pearlitic steel and α-iron. *Mater. Sci. Eng. A*, 2007, **452-453**, 633-639.
doi*:* 10.1016/j.msea.2006.11.147.

20. Ungar, T.; Dragomir, I.; Revesz, A. & Borbely, A. The contrast factors of dislocations in cubic crystals: the dislocation model of strain anisotropy in practice. *J. Appl. Crystallography*, 1999, **32**, 992-1002.
doi*:* 10.1107/S0021889899009334.

21. Dragomir, I.C. & Ungar. T. The dislocations contrast factors of cubic crystals in the Zener constant range between zero and unity. *Powder Diffraction,* 2002, **17**(2), 104-111.
doi:10.1154/1.1471520.

22. Martinez-Garcia, J.; Leoni, M. & Scardi, P. Analytical expression for dislocation contrast factor of ‹011›, {100} cubic slip system: Application to $Cu_2O$. *Physical Review B*, 2007, **76**, 174117, 1-8.

23. Yadav, R. A. Establishment of a spring formula for low temperature use of spring. *Def. Sci. J.*, 1974, **25**, 69-76.
doi: 10.14429/dsj.25.6596.

24. Chatterjee, D.P. Steels in Ordnance Factories. *Def. Sci. J.*, 1960, **10**(2A), 40-44.
doi: 10.14429/dsj.10.7651

## CONTRIBUTORS

**Mr Shamsher Singh Bargujer** did his BTech (Mechanical Engineering) from Regional Engineering College, Kurukshetra, in 1997 and ME (Thermal Engineering) from Delhi College of Engineering, Delhi, in 1999. Currently pursuing his PhD in Production Engineering from PEC University of Technology, Chandigarh. Presently, he is working as Assistant Works Manager and Divisional Officer of quality control at Ordnance Cable Factory, Chandigarh. He worked in area of defence production, planning and quality control since 2002. All experimentation in this study is carried out by him and manuscript compiled by him.

**Dr Narender M. Suri** did his graduation in Production Engineering from GBP University of Technology, Pantnagar, in 1990 and post-graduation in Industrial Metallurgy from IIT, Roorkee, in 1995. Obtained his PhD in Welding Engineering from IIT, Delhi in 2005. Presently, he is the head of Production engineering department. His area of specialisation is welding engineering,

casting technology, material science and operation research. He has published more than 20 research paper in international and national journals. He is member of ISTE. He carried out analysis of XRD diffraction peaks. He also carried out detail discussion on results and concluded the manuscript.

**Dr Rajendra M. Belokar** did his graduation from Amravati University, Amravati, in 1987. He did post-graduation and PhD from PEC University of Technology, Chandigarh, in 1999 and 2010 respectively. Presently, he is associate professor in Production Engineering, PEC University ofTechnology, Chandigarh. He published more than 70 research papers in national and international journals. He published one book and two books are in press. He is Sr. Member SME (USA), M.I.E, C. Eng (I), LM-ISTE, Member-INVEST, and Member APICS (USA). He framed the manuscript and plotted all relevant plots in the manuscript.